ORIGINAL ARTICLE

Finite element simulation of machining of Ti-6Al-4V alloy with thermodynamical constitutive equation

Fang Shao · Zhanqiang Liu · Yi Wan · Zhenyu Shi

Abstract Titanium alloys are known as difficult-to-machine materials, especially at higher cutting speeds, due to their several inherent properties such as low thermal conductivity and their high reactivity with cutting tool materials, which present a low thermal conductivity. In this paper, a finite element analysis (FEA) of machining for Ti-6Al-4V is presented. In particular, the thermodynamical constitutive equation in FEA is applied for both workpiece material and tool material. Cutting temperature and tool wear depth are predicted. The comparison between the predicted and experimental cutting temperature and tool wear depth are presented and discussed. The results indicated that a good prediction accuracy of both principal cutting temperature and tool wear depth can be achieved by the method of FEA with thermodynamical constitutive equation.

Keywords Ti-6Al-4V · Finite element analysis · Thermodynamical constitutive equation

1 Introduction

Ti-6Al-4V alloy is one of the most important engineering alloys for combining attractive properties with inherent workability [1–4]. Many studies on finite element (FE) simulation of Ti-6Al-4V alloy machining have been published until now, especially on machining in high-speed

F. Shao (✉) · Z. Liu · Y. Wan · Z. Shi
School of Mechanical Engineering, Shandong University,
Jinan 250061, China
e-mail: bzshaofang999@163.com
URL: binzhouvacational.com

F. Shao
Binzhou Vacational College,
Binzhou 256603, China

machining. High-speed machining processes are of growing industrial interest [5] not only because they allow for larger material removal rates but also because they may positively influence the properties of the finished workpiece [6].

Domenico Umbrello presented a finite element analysis (FEA) of machining of TiAl6V4 both for conventional and high-speed cutting regimes. In particular, cutting force, chip morphology, and segmentation are taken into account due to their predominant roles to determine machinability and tool wear during the machining of these alloys. Songwon Seo et al. attained a high-temperature split Hopkinson's pressure bar (SHPB) test system using two ellipsoidal radiant heating reflectors with two halogen lamps to investigate the effects of temperature for the titanium alloy Ti-6Al-4V. Some researches [7–11] showed that the success and reliability of numerical models are heavily dependent upon work material flow stress, friction parameters between the tool and work material interfaces, the fracture criterion, and the thermal parameters. In other words, it depends on the choice of appropriate constitutive equations.

Titanium and its alloys are especially an important class of aerospace engineering materials due to their excellent combination of strength and fracture toughness as well as low density. However, these materials are regarded as difficult to machine because of their low thermal conductivity and high chemical reactivity with cutting tool materials. Moreover, the low thermal conductivity of titanium inhibits dissipation of heat within the workpiece causing an higher temperature at the cutting edge and generating for higher cutting speed, a rapid chipping at the cutting edge which leads to catastrophic failure.

In order to increase productivity and tool life in the machining of titanium alloys, it is necessary to develop a reliable FE model for conventional cutting speed regime and, especially, for high-speed machining.
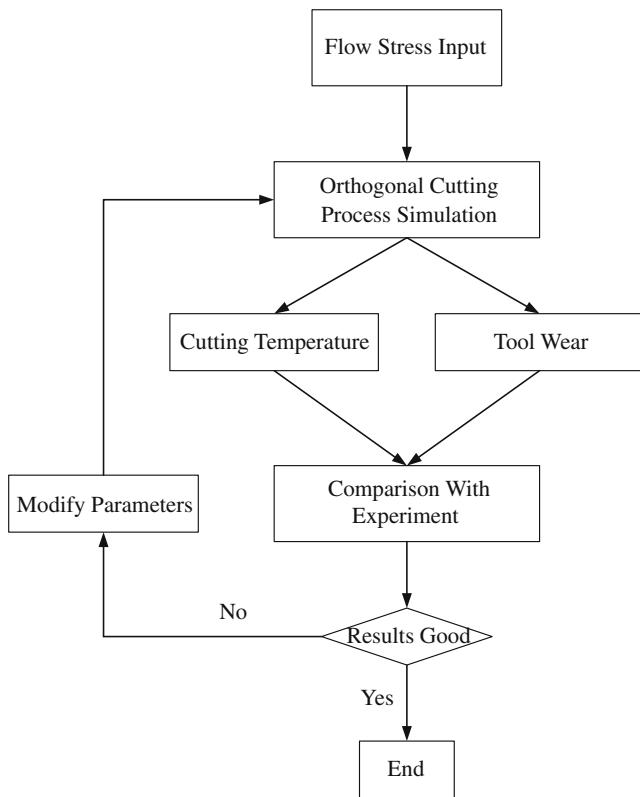
Fig. 1 Flow chart of the tool wear calculation

In recent years, the Johnson–Cook's constitutive equation is always used as a finite element model to simulate orthogonal cutting of Ti-6Al-4V alloy. Although such model is widely used in finite element simulations to describe the constitutive behavior of metals at high strain rates over a wide range of temperatures, its applicability over a wide range of strain is, however, limited due to the use of SHPB method that permits to achieve only a limited range of strains.

Tool wear is subject to factors of vary nonlinearity and strong coupling function, and the thermodynamics provides
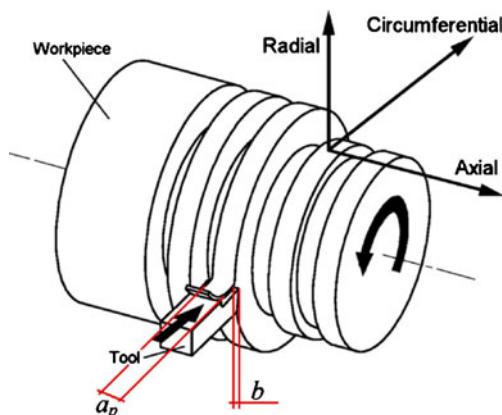

Fig. 2 Configuration of the orthogonal cutting tests

Table 1 Chemical composition of Ti-6Al-4V

Element	Al	Ti	V	Fe/O
Component (wt.%)	6	90	4	Max 0.2

a multifactor analysis method of nonlinear interaction, so using the theory and methods of thermodynamics to study the friction and wear process is reasonable and feasible [12]. However, little literature on researches of tool wear based on thermodynamics constitutive mechanism is reported until now. The aim of this study is to deduce the thermodynamical constitutive equation (T-C-E) of Ti-6Al-4V alloy at high temperature, which is used to build an orthogonal FE model during high-speed machining of Ti-6Al-4V alloy.

2 Simulation

Figure 1 shows the flow chart of the tool wear calculation program. The program is designed to perform tool wear calculation automatically step by step until a tool reshape criterion is reached. In every calculation loop, chip formation and heat transfer analysis jobs are submitted to analyze the steady-state cutting process and obtain the cutting process variable values necessary for the calculation of wear rate at steady state. If the results are not satisfied, a second tool wear calculation loop starts with the updated tool geometry. The flow chart is presented in Fig. 1.

The simulated cutting conditions are identical to those of the experiments performed on numerically controlled lathe utilizing a radial feed (Fig. 2) at cutting speeds (v) of 200 m/min, uncut chip thickness (b) of 0.14 mm, and width of cut(a_p) of 0.5 mm. The cutting temperature (along the rake face in Fig. 2) was measured using an infrared thermal imager, and the tool wear depth was measured using a white-light interferometer.

The chemical composition of workpiece material is shown in Table 1. The mechanical and physical properties

Table 2 Mechanical and physical properties of Ti-6Al-4V

Density	$4.43 \times 10^3 \text{kg/m}^3$
Ultimate tensile strength (MPa)	950
Tensile yield strength (MPa)	880
Modulus of elasticity (GPa)	113.8
thermal conductivity (W/(m K))	17
Poisson's ratio	0.342
Heat capacity (J/kg K)	526

Table 3 Mechanical and physical properties of tool material WC-Co

Density	$14.5 \times 10^3 \text{kg/m}^3$
Ultimate tensile strength (MPa)	3,000
Modulus of elasticity (GPa)	650
thermal conductivity (W/(m K))	58.9888
Poisson's ratio	0.25
Heat capacity (J/kg K)	15.0018

of workpiece material and tool material are also presented in Tables 2 and 3, respectively. The cutting tool geometry for WC CNMA432 consisted of a normal rake angle and a normal flank angle of 15° and 6°, respectively. The tool cutting edge angle is 90°, the tool cutting edge inclination angle is 0°, and the tool cutting edge radius is of 0.030 mm. No cutting fluid was used in the tests.

2.1 Numerical model of orthogonal machining

The commercial FEA software DEFORM-3D, a Lagrangian implicit code, is used to simulate the orthogonal cutting process of Ti-6Al-4V titanium alloy. FEM model of the orthogonal cutting process is developed that the tool is no longer modeled as rigid (Fig. 3). The workpiece is initially meshed with 8,000 isoparametric quadrilateral elements, while the tool is modeled as nonrigid and meshed and subdivided into 1,000 elements (Fig. 4). A plane-strain coupled thermomechanical analysis is performed using orthogonal assumption.

2.2 Material modeling

To model the thermo-elastoplastic behavior of workpiece material titanium alloy Ti-6Al-4V and tool material WC-
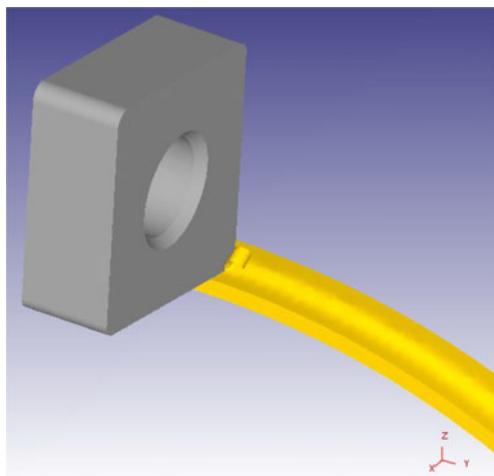
Co, the J–C constitutive equation is initially employed, which can be represented by the following equation [13]:

$$\sigma = (A + B\varepsilon^n)(1 + C\ln\dot{\varepsilon})\left[1 - \left(\frac{T - T_{\text{room}}}{T_{\text{melt}} - T_{\text{room}}}\right)^m\right] \quad (1)$$

where σ is the flow stress, ε is the plastic strain, $\dot{\varepsilon}$ is the strain rate (per second), $\dot{\varepsilon}_0$ is the reference plastic strain rate (per second), T (degree Celsius) is the workpiece temperature, T_{melt} (1,668°C) is the melting temperature of the workpiece material, and T_0 (20°C) is the room temperature. Coefficient A (megapascals) is the yield strength; B (megapascals) is the train hardening modulus; C is the strain rate sensitivity coefficient; n is the hardening coefficient; m is the thermal softening coefficient. Table 4 reports the material constants obtained by the researcher [13].

Taking above values into Eq. 1, the J–C model of workpiece material and tool material are represented as:

$$\sigma = (782.7 + 498.4\varepsilon^{0.28})(1 + 0.028\ln\dot{\varepsilon})$$
$$\times \left[1 - \left(\frac{T - 20}{1,648}\right)\right] \quad (2)$$

$$\sigma = (0.003 + 8.0471\varepsilon^{0.0003})\left[1 - \left(\frac{T - 20}{1,352}\right)^{0.179}\right] \quad (3)$$

In order to rich the high-speed machining theories, the thermodynamics constitutive equation which is expressed as Eq. 4 [14] is deduced and is used in this paper.

$$\sigma = \left(B\varepsilon_p^n\right)\left(1 + B_1 T[\dot{\varepsilon}_P]^{\frac{1}{m}} - B_2 T e^{A\left(1 - \frac{T}{T_t}\right)}\right) + Y_a \quad (4)$$

where A, B, B_1, B_2, n, m, and Y_a are seven constants associated with material.


Fig. 3 Tool and workpiece
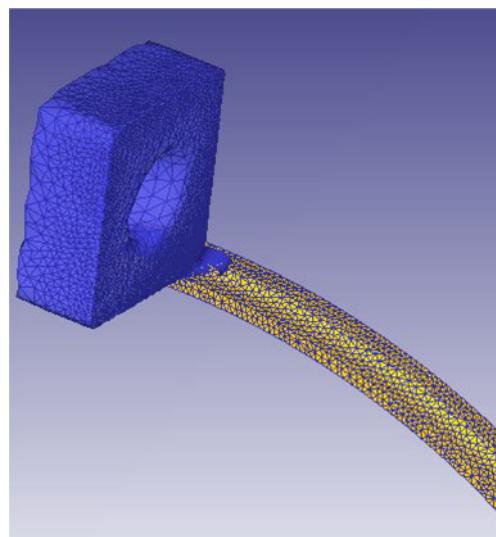
Fig. 4 Meshed tool and workpiece

Table 4 The material constants of workpiece material Ti-6Al-4V and tool material WC-Co

Constant	A	B	C	n	m	T_{room} (°C)	T_{melt} (°C)
Ti-6Al-4V	782.7	498.4	0.028	0.28	1	20	1,668
WC-Co	0.003	8.0471	0.000	0.0003	0.179	20	1,372

Equations 2 and 3 should be fitted to Eq. 4 with least square method to become thermodynamical constitutive equation. Two MATLAB programs are compiled in order for solving the seven fitting parameters of the thermodynamical constitutive equation.

So, take the results from MATLAB programs into Eq. 4, the last thermodynamical constitutive equations for workpiece material and tool material are obtained as:

$$\sigma = \left(0.5864\varepsilon_p^{0.2796}\right)\left(1 + 0.1T[\dot{\varepsilon}_P]^{10} + 0.8Te^{-0.1008\left(1-\frac{T}{T_t}\right)}\right) + 365.5 \tag{5}$$

$$\sigma = \left(2.029\varepsilon^{0.2735}\right)\left(1 + 0.0001T[\dot{\varepsilon}_p]^{\frac{1}{0.0001}} - 0.6906Te^{0.3047\left(1-\frac{T}{1372}\right)}\right) + 2.1 \tag{6}$$

To validate the orthogonal cutting model, the predicted and experimentally measured cutting temperature and tool wear depth were compared and their differences were discussed.

2.3 Cutting temperature

Table 5 gives the experimental temperature and predicted temperature (the distance is 0.05 mm between tool rake face and chip edge). The comparison between the experimental and the predicted temperature obtained by the application of the T-C-E model are shown in Table 5 and Fig. 5, respectively.

It is obvious that tendency of the predicted cutting temperature found by the application of the T-C-E are almost similar to the experiment in Figs. 6, 7, 8, and 9. This result permits to assess that the assumption of the T-C-E model used in the present study appears to be reasonable.

2.4 Tool wear

With this tool wear estimation program, tool wear progress under the same turning cutting conditions as described in Table 6 is calculated. The predicted results can be seen in Figs. 10, 11, 12, and 13.

The comparison between the experimental and the predicted tool wear depth obtained by the application of the T-C-E model is shown in Table 6 and Fig. 14. The solid line in Fig. 14 shows the wear progress curves of crater wear obtained from experiment under the same cutting condition. The dot lines are the predicted tool wear curves. It is found that the estimated crater wear is smaller than experimental ones. In experiment, after 60 s of cutting, the crater wear has exceeded 0.15 mm, while after 120 s, the estimated crater wear just arrives at 0.18 mm.

The discrepancy may be caused by:

1. The simplified and low coefficient of friction. In the chip formation analysis, Coulomb's friction model is adopted and a constant coefficient of friction 0.3 is used in the whole tool wear estimation process. According to the verification of chip formation analysis in continuous chip formation, the predicted cutting force and thrust force are smaller than the experimental data by about 15% and 35% when the coefficient of friction is set to 0.3. This maybe means that the predicted variables for the calculation of tool wear have error as well. Therefore, chip formation modeling is very important for the accuracy of tool wear estimation. In order to improve the prediction, it is expected that in the later tool wear estimation, the coefficient of friction should be calculated according to the cutting force and tool geometry or with a more reliable method.

2. Inconsistencies of material combination. Because the characteristic equations of tool wear and the tool wear data come from different literatures and researchers, it is

Table 5 The experimental temperature and predicted temperature (the distance is 0.05 mm between tool rake face and chip edge)

Cutting time (s)	1	60	120	180
Step	531,915	1.6e7	3.2e7	6.4e7
Experimental temperature (°C)	132.5	259.2	589.9	650.4
Predicted temperature (°C)	130	360	800	950
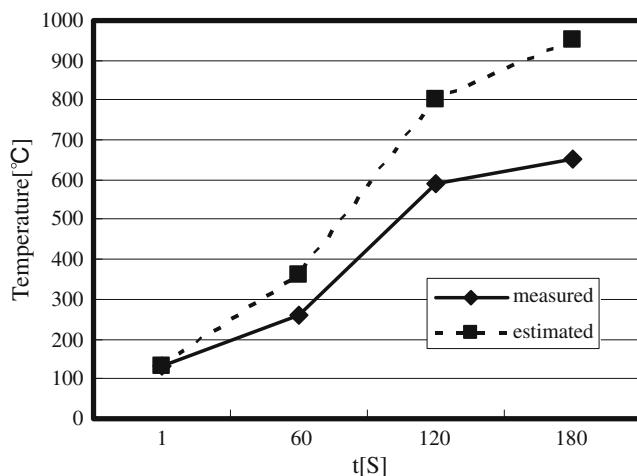
Fig. 5 Comparison between estimated and experimental progress curves for tool temperature (under cutting condition: v_c=200 m/min, a_p=0.5 mm, f=0.14 mm/r)
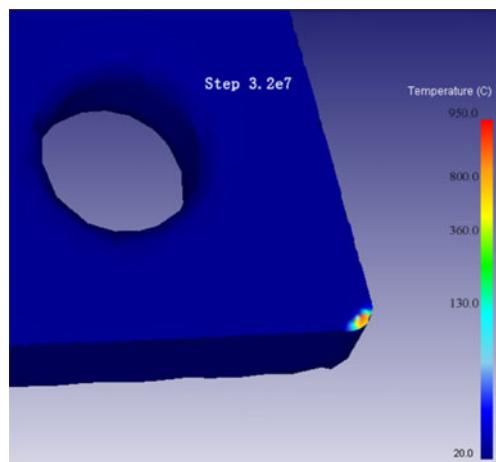

Fig. 8 Predicted temperature (t=120 s)
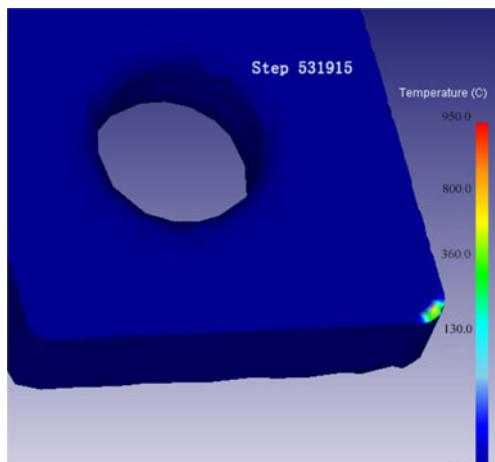
Fig. 6 Predicted temperature (t=1 s)
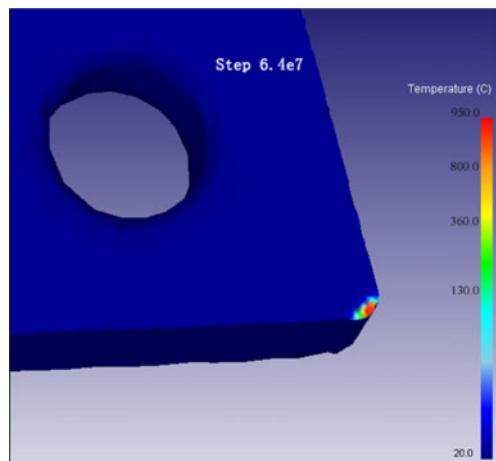

Fig. 9 Predicted temperature (t=180 s)
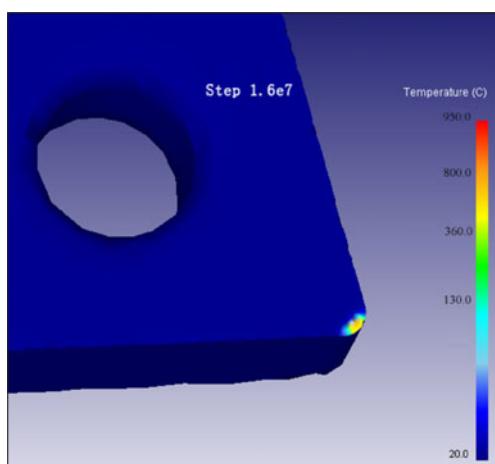
Fig. 7 Predicted temperature (t=60 s)

Table 6 Experimental tool wear depth and predicted tool wear depth

Cutting time (s)	1	60	120	180
Step	531,915	1.6e7	3.2e7	6.4e7
Experimental tool wear depth (mm)		0.017	0.15	0.362
Predicted tool wear depth (mm)	0.015	0.09	0.18	0.36
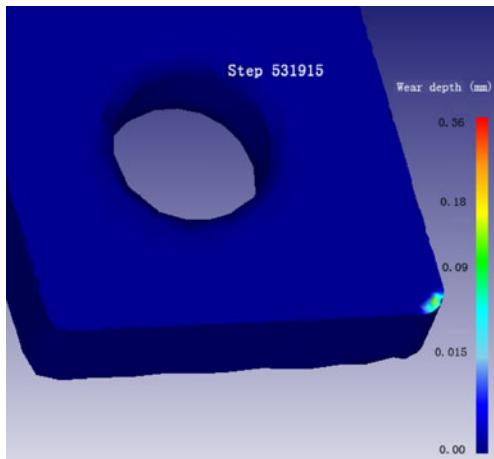
Fig. 10 Predicted tool wear depth (t=1 s)
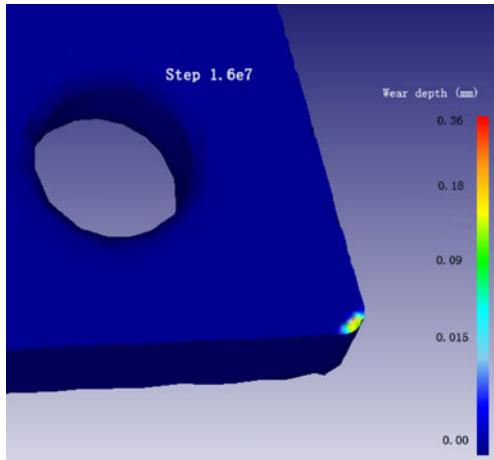
Fig. 11 Predicted tool wear depth (t=60 s)
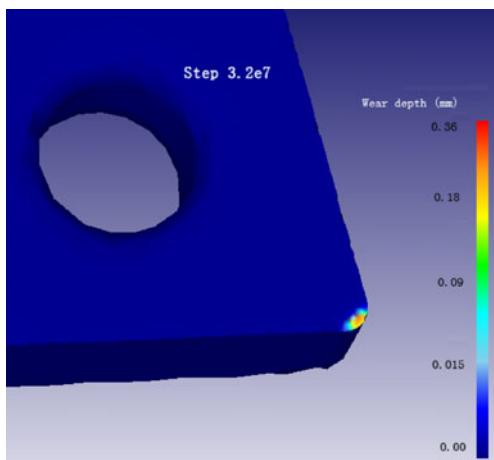
Fig. 12 Predicted tool wear depth (t=120 s)
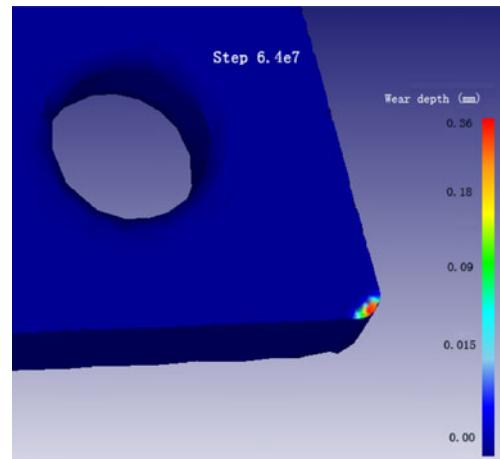
Fig. 13 Predicted tool wear depth (t=180 s)

unavoidable that differences exist in these tool and workpiece material's chemical composition and structure. It was tested by Kitagawa et al. that the content and size of abrasive particle dispersed in workpiece material and chemical composition of tool material could be correlated with change in the constants of the wear characteristic equation both in higher and lower temperature ranges [15].

3. Contact between flank wear and the workpiece. From Fig. 9, after a certain tool wear is formed, wear rate on rake face is decreasing and the wear rate on flank face decreases more than that on rake face. It is observed that the temperature on crater wear drops off to a low value. This may be caused by the poor contact between crater wear and the workpiece.

In order to obtained more accuracy simulation results, the Coulomb friction coefficient used in the Deform 3D
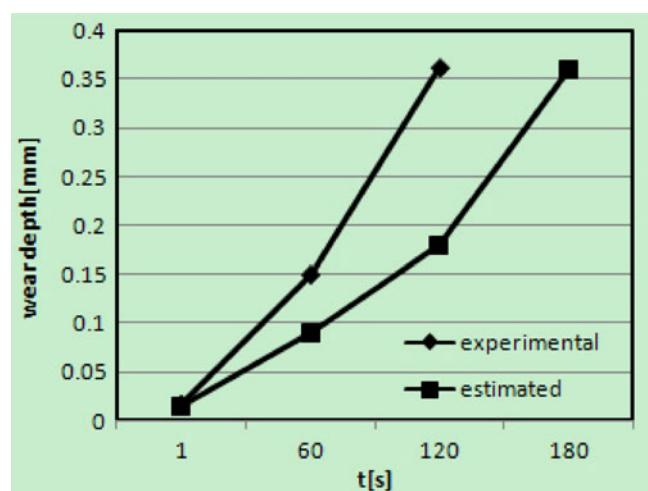

Fig. 14 Comparison between estimated and experimental progress curves for tool wear (under cutting condition: v_c=200 m/min, a_p=0.5 mm, f=0.14 mm/r)

Table 7 The experimental temperature and predicted temperature (using modified friction model: f=0.7, v=300 m/min)

cutting time (s)	1	60	120	180
Step	531,915	1.6e7	3.2e7	6.4e7
Experimental temperature (°C)		136.0	370.2	835.5	970.8
Predicted temperature (°C)		140	390	870	1,035
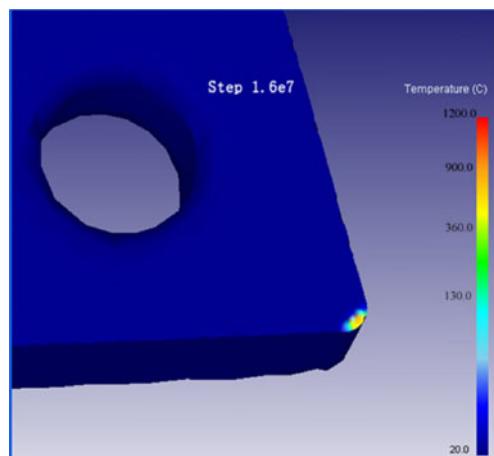
Fig. 16 Predicted modified temperature (t=60 s)

Table 8 Experimental tool wear depth and predicted tool wear depth (using modified friction model: f=0.7, v=300 m/min)

Cutting time (s)	1	60	120
Step	531,915	1.6e7	3.2e7
Experimental tool wear depth (mm)		0.017	0.155	0.368
Predicted tool wear depth (mm)		0.015	0.17	0.39
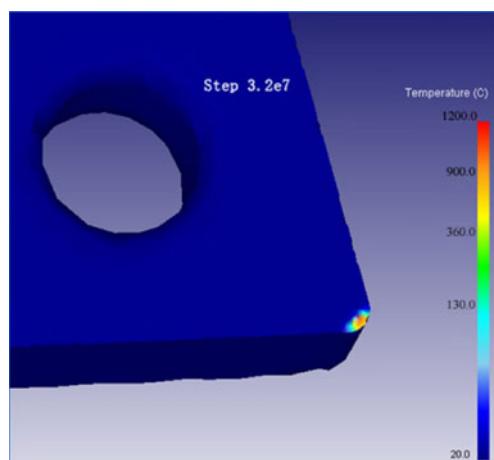
Fig. 17 Predicted modified temperature (t=120 s)
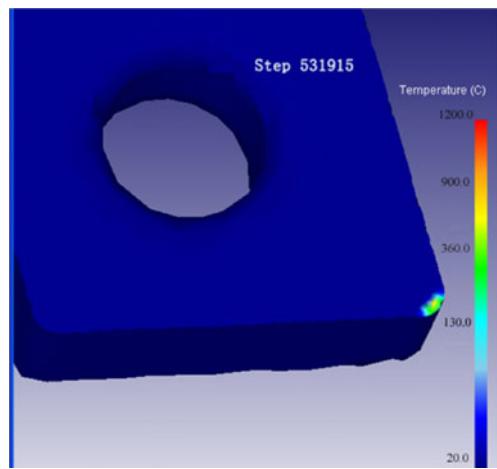
Fig. 15 Predicted modified temperature (t=1 s)
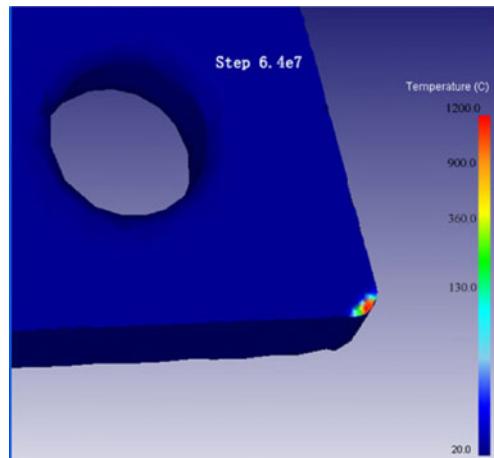
Fig. 18 Predicted modified temperature (t=180 s)
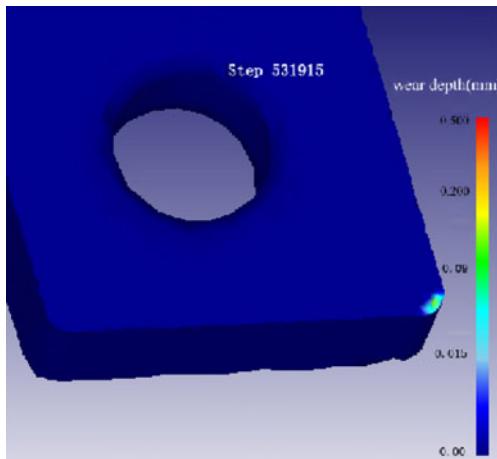
**Fig. 19** Predicted modified tool wear depth ($t=1$ s)
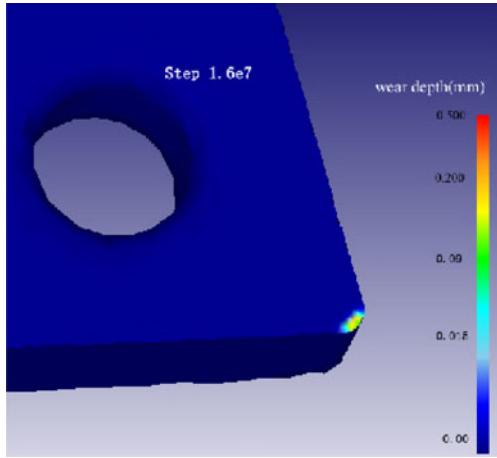
Fig. 20 Predicted modified tool wear depth ($t=60$ s)
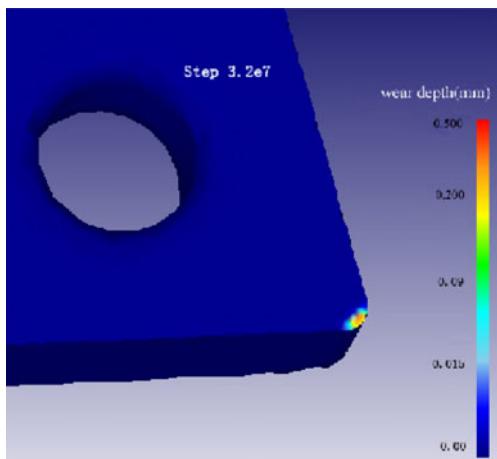
**Fig. 21** Predicted modified tool wear depth ($t=120$ s)
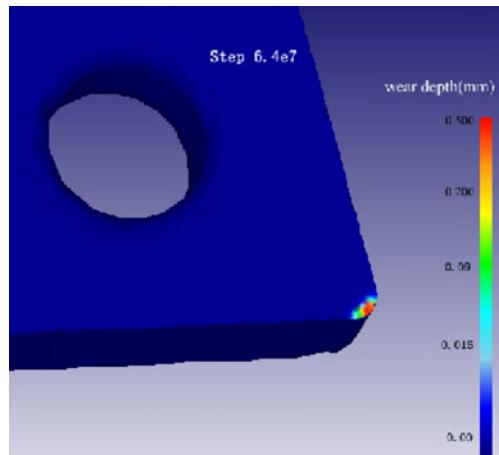
Fig. 22 Predicted modified tool wear depth ($t=180$ s)
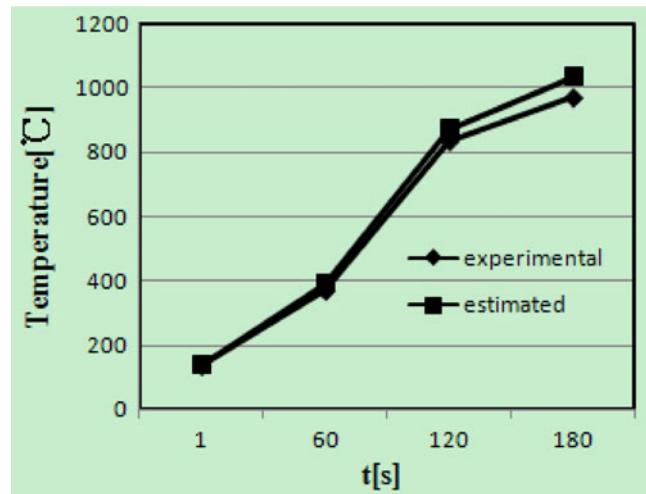

Fig. 23 Comparison between estimated and experimental progress curves for tool temperature (under cutting condition: $v_c=300$ m/min, $a_p=0.5$ mm, $f=0.14$ mm/r)
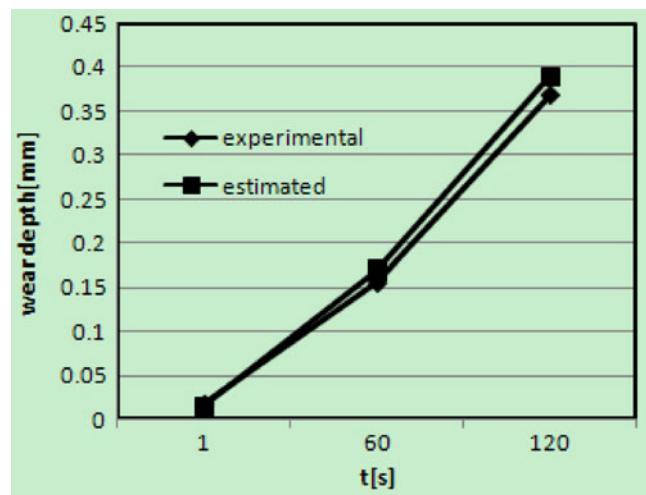

Fig. 24 Comparison between estimated and experimental progress curves for tool wear (under cutting condition: $v_c=300$ m/min, $a_p=0.5$ mm, $f=0.14$ mm/r)

model is modified as 0.7; simultaneously, the cutting speed is increased to 300 m/min, the simulation temperature and tool wear depth are presented in Tables 7 and 8 and Figs. 15, 16, 17, 18, 19, 20, 21, and 22, and the comparisons between experimental and estimated results are presented in Figs. 23 and 24.

Errors are all less than 10% as shown in Figs. 23 and 24. The results indicated that a good prediction accuracy of both principal cutting temperature and tool wear depth can be achieved by the method of FEA with thermodynamical constitutive equation.

3 Conclusion

A FEA of machining for Ti-6Al-4V is presented. In particular, the T-C-E in FEA is applied for both work piece material and tool material. Research results indicated that a reasonable prediction of temperature and tool wear depth is obtained when using model T-C-E in high-speed machining. These evidences permit to establish that good numerical results can be obtained when simulating cutting conditions similar to those utilized to characterize material constitutive law. Therefore, it can be concluded that the T-C-E model in this paper can be employed to study the orthogonal process of Ti-6Al-4V alloy and to predict the reality of the temperature and tool wear depth with satisfactory accuracy.

References

1. Umbrello D (2008) Finite element simulation of conventional and high speed machining of Ti6Al4V alloy. J Mater Process Technol 196:79–87
2. Seo S, Min O, Yang H (2005) Constitutive equation for Ti–6Al–4V at high temperatures measured using the SHPB technique. Int J Impact Eng 31:735–754
3. Rittel D, Wang ZG (2008) Thermo-mechanical aspects of adiabatic shear failure of AM50 and Ti6Al4V alloys. Mech Mater 40:629–635
4. Lee W-S, Lin C-F (1998) High-temperature deformation behaviour of Ti6Al4V alloy evaluated by high strain-rate compression tests. J Mater Process Technol 75:127–136
5. Schulz H (ed) (2001) Scientific fundamentals of HSC. Hanser, München
6. Tönshoff H-K, Hollmann F (eds) (200) Spanen Metallischer Werkstoffe bei hohen Geschwindigkeiten. Deutsche Forschungsgemeinschaft
7. Childs THC (1998) Material property needs in modeling metal machining. Proceedings of the CIRP International Workshop on Modeling of Machining Operations, Atlanta, GA, 19, pp 193–202
8. Trent EM (1988) Metal cutting and the tribology of seizure: I seizure in metal cutting. Wear 128:29–45
9. Shaw MC (2005) Metal cutting principles, 2nd edn. Oxford Science, Oxford, p 651
10. Childs THC, Maekawa K, Obinakawa T, Yamane Y (2000) Metal machining—theory and applications. Elsevier, Amsterdam, p 408
11. Astakhov VP (1999) Metal cutting mechanics. CRC, Boca Raton
12. Dai Z, Wang M, Xue Q (2002) Introduction to Tribothermodynamics. National Defence Industry, Beijing
13. Zhanqiang L, Jihua W, Zhenyu S, Pifen Z (2008) State-of-the-art of constitutive equations in metal cutting operations. Tools Technol 42:3–9
14. Voyiadjis GZ, Almasri AH (2008) A physically based constitutive model for fcc metals with applications to dynamic hardness. Mech Mater 40:549–563
15. Kitagawa T, Maekawa K, Shirakashi T, Usui E (1988) Analytical prediction of flank wear of carbide tools in turning plain carbon steels, part 1: characteristic equation of flank wear. Bull Jpn Soc Precis Eng 22:263–269